On the Dynamics and Water Mass Transformation of a Boundary Current Connecting Alpha and Beta Oceans

ERWIN LAMBERT

Geophysical Institute, University of Bergen, and Bjerknes Centre for Climate Research, Bergen, Norway, and Institute for Marine and Atmospheric Research Utrecht, Utrecht University, Utrecht, Netherlands

TOR ELDEVIK

Geophysical Institute, University of Bergen, and Bjerknes Centre for Climate Research, Bergen, Norway

MICHAEL A. SPALL

Department of Physical Oceanography, Woods Hole Oceanographic Institution, Woods Hole, Massachusetts

(Manuscript received 14 September 2017, in final form 13 July 2018)

ABSTRACT

A subpolar marginal sea, like the Nordic seas, is a transition zone between the temperature-stratified subtropics (the alpha ocean) and the salinity-stratified polar regions (the beta ocean). An inflow of Atlantic Water circulates these seas as a boundary current that is cooled and freshened downstream, eventually to outflow as Deep and Polar Water. Stratification in the boundary region is dominated by a thermocline over the continental slope and a halocline over the continental shelves, separating Atlantic Water from Deep and Polar Water, respectively. A conceptual model is introduced for the circulation and water mass transformation in a subpolar marginal sea to explore the potential interaction between the alpha and beta oceans. Freshwater input into the shelf regions has a slight strengthening effect on the Atlantic inflow, but more prominently impacts the water mass composition of the outflow. This impact of freshwater, characterized by enhancing Polar Water outflow and suppressing Deep Water outflow, is strongly determined by the source location of freshwater. Concretely, perturbations in upstream freshwater sources, like the Baltic freshwater outflow into the Nordic seas, have an order of magnitude larger potential to impact water mass transports than perturbations in downstream sources like the Arctic freshwater outflow. These boundary current dynamics are directly related to the qualitative stratification in transition zones and illustrate the interaction between the alpha and beta oceans.

1. Introduction

The Nordic seas play a crucial role in the global ocean, as they connect the North Atlantic to the Arctic Ocean. Oceanic transports of mass, heat, and salt through this marginal sea complete the global thermohaline circulation (e.g., Kuhlbrodt et al. 2007) and the global hydrological cycle (e.g., Haine et al. 2015). Because of its placement, the Nordic seas reside between the subtropics, where temperature dominates stratification (the alpha ocean), and the polar regions, where salinity dominates stratification (the beta ocean; Carmack 2007). The Nordic seas are a transition zone (Sverdrup et al. 1942; Stewart and Haine 2016) where both temperature and salinity contribute significantly to stratification. In this study, we illustrate that this relatively rare density structure introduces novel dynamics governing the circulation and water mass transformation in a marginal sea.

The Nordic seas (Fig. 1) host significant water mass transformation of Atlantic Water (AW) through net cooling and freshening. As AW enters the marginal sea across the Greenland–Scotland Ridge, it is transformed into both denser and lighter water masses which largely exit the Nordic seas across the same gateway

Denotes content that is immediately available upon publication as open access.

Corresponding author: Erwin Lambert, erwin.lambert@uib.no

DOI: 10.1175/JPO-D-17-0186.1

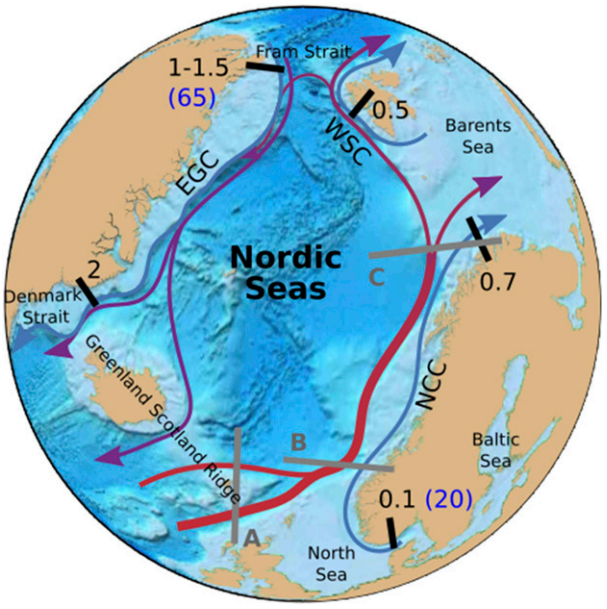

FIG. 1. The Nordic seas and schematic circulation. Black numbers are the observed transport of low-salinity water masses (Sv), which in this study collectively are referred to as PW. Blue numbers are observed freshwater fluxes from the Baltic and the Arctic Ocean (mSv). NCC, Norwegian Coastal Current; WSC, West Spitsbergen Current; EGC, East Greenland Current. Locations of observations are approximate; literature on volume and freshwater transports is cited in the introduction. Gray lines indicate sections shown in Fig. 2.

(e.g., Hansen and Østerhus 2000). We will refer to the dense water masses collectively as Deep Water (DW; cold) and to the light water masses as Polar Water (PW; fresh). DW is commonly defined as having a potential density above 27.8 kg m^{-3} and PW as having a salinity below a threshold of, for example, 34.5 g kg^{-1} (Eldevik and Nilsen 2013). From the latter criterion, both cold fresh coastal waters (like in the East Greenland Current) and those of higher temperature (like in the Norwegian Coastal Current; cf. Fig. 1) will be classified as PW herein.

The circulation including both an increase and a decrease of density is termed a double estuarine circulation, as it connects an overturning and an estuarine circulation through a shared inflow (Stigebrandt 1985; Rudels 2010). Hansen and Østerhus (2000) quantified this circulation in the Nordic seas, estimating that approximately 6 out of 8.5 Sv (1 Sv $\equiv 10^6$ m^3 s^{-1}) of Atlantic inflow returns as a denser water mass and the resulting 2.5 Sv as a lighter water mass. Previous studies have argued that the strength of the Atlantic inflow, which feeds the double estuarine circulation, may be partly controlled by the water mass transformation within the Nordic seas (Spall 2012; Eldevik and Nilsen 2013; Lambert et al. 2016).

The transformation of AW that results in a net density increase occurs primarily in the boundary current as postulated by Mauritzen (1996), who attributed this transformation to surface heat loss from the boundary region. Spall (2004) indicated that lateral heat loss from the boundary due to eddy fluxes could contribute significantly to net densification. The downstream buoyancy loss can induce a shoreward flow onto the continental shelves, forming a barotropic coastal current (Walin et al. 2004). In addition, the downstream densification of AW can lead to a more barotropic boundary current as waters sink, leading to an actual overturning in the meridional-vertical plane (Straneo 2006). This downstream modification of a warm, saline boundary current, inducing a net density increase through heat loss, is the current theory for the overturning circulation in the Nordic seas (Mauritzen et al. 2011). We postulate also that the transformation resulting in a net density decrease (estuarine circulation) can be described as a downstream transformation of the boundary current.

The production of a low-salinity (low-density) water mass in the Nordic seas can be traced upstream to the emergence of the Norwegian Coastal Current (see Fig. 2). From the Baltic, a fresh outflow of approximately 0.1 Sv enters the perimeter of the Nordic seas near the Atlantic inflow (Winsor et al. 2001; see Fig. 1 herein). This Baltic outflow establishes a halocline and a buoyant coastal current which strengthens downstream. At the Barents Sea Opening, volume transports of this low-salinity water mass are estimated at 0.7 Sv (Blindheim 1989; Björk et al. 2001; Skagseth et al. 2011). A qualitatively similar coastal current carries 0.5 Sv of low-salinity water along the West Spitsbergen Current (Walczowski 2013), and at the latitude of the Fram Strait, 1–1.5 Sv of PW flows equatorward alongside modified AW (Björk et al. 2001; de Steur et al. 2014). Along the coast of Greenland, the composition of water masses carried by the East Greenland Current changes further with an increase in PW transport (Håvik et al. 2017) before it exits the Nordic seas through the Denmark Strait. At this gateway, the outflow of PW from the Nordic seas is estimated at 2 Sv (Sutherland and Pickart 2008; de Steur et al. 2017). Based on these estimates, we hypothesize that a significant amount of PW is produced as a downstream strengthening coastal current originating at the Baltic–North Sea opening.

PW formation is typically attributed to processes in the Arctic Ocean (e.g., Stigebrandt 1981; Rudels 1989). These processes are often considered to be limited by vertical mixing across the basinwide halocline (e.g., Nilsson and Walin 2010; Spall 2013). However, considerable evidence exists of PW being formed in the margins

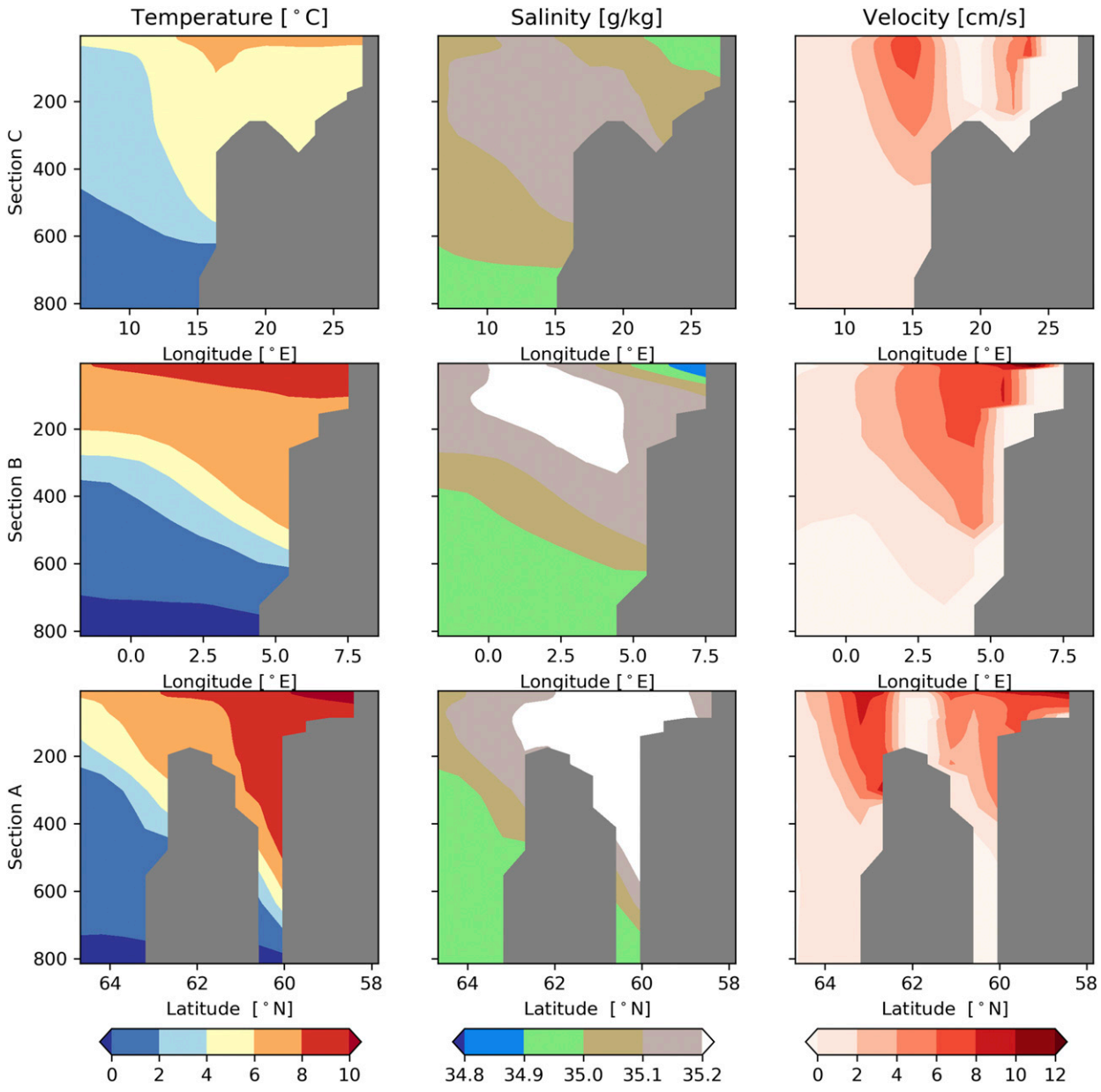

FIG. 2. Hydrography across the Nordic seas boundary current. (left) Average temperature, (center) salinity, and (right) along-boundary velocity across three sections in the eastern Nordic seas from the Estimating the Circulation and Climate of the Ocean (ECCO) reanalysis product between 1992 and 2015 (Forget et al. 2015; Fukumori et al. 2017). The sections correspond to the gray lines in Fig. 1. Section A is similar to standard sections north and south of the Faroe Islands, section B is similar to the standard Svinøy section, and section C is similar to the standard Gimsøy section.

of the Nordic seas due to processes related to the observed coastal current (Bacon et al. 2008). These processes include wind stress (Whitney and Garvine 2005; St-Laurent et al. 2012), sea ice melt in the marginal ice zone (Boyd and D'Asaro 1994; Steele et al. 1995), eddy fluxes (Spall 2013; St-Laurent et al. 2012), and double diffusion (Cottier and Venables 2007). Based on observations across the West Spitsbergen Current, Saloranta and Haugan (2004) concluded that observed PW formation can only be described realistically if significant diapycnal exchange is accounted for. The abovementioned processes are ultimately dependent on the presence of a freshwater source maintaining salinity stratification.

A number of conceptual studies have addressed the role of combined heat loss and freshwater input into a marginal sea such as the Nordic seas.

Spall (2012) concluded that interior freshwater input can weaken the circulation of AW by reducing the density contrast between the boundary current and the interior and that sufficient interior freshwater input can induce an abrupt transition. However, the bulk of freshwater input into the Nordic seas enters the shelf regions. This freshwater input is dominated by three sources: runoff from the Norwegian and Greenland coasts (20 mSv; Dickson et al. 2007), freshwater outflow from the Baltic (20 mSv; Winsor et al. 2001), and liquid freshwater outflow from the Arctic (65 mSv; de Steur et al. 2014). Using a box model, Lambert et al. (2016) indicated that the impact of freshwater input on the circulation of AW depends strongly on the distribution of freshwater input between dense waters in the interior and buoyant waters as found in the coastal regions. Including a coastal freshwater source, Wåhlin and Johnson (2009) showed that the downstream density modification of an AW boundary current due to combined heat loss and freshwater input depends on the adjustment length scales of temperature and salinity. If cooling of AW occurs over shorter length scales than freshening, a density maximum is formed between inflow and outflow. However, the question of how this impacts the circulation strength was left unanswered.

The above studies rely on the a priori assumption that stratification in the boundary region is dominated by a single tracer. Although Wåhlin and Johnson (2009) allowed for either temperature or salinity to dominate stratification at each point along the boundary, they did not allow for both temperature and salinity to dominate stratification. The observed presence of a buoyant coastal current alongside the Atlantic boundary current in the Nordic seas, and the significant downstream formation of a low-salinity water mass in its margins, requires an enhanced description of AW transformation beyond that of a single dominating tracer. Instead, we must describe the Nordic seas as a transition zone. Temperature stratification (the alpha ocean) maintains a thermocline that divides AW from interior waters, and salinity stratification (the beta ocean) maintains a halocline over the continental shelves (see Fig. 2). These pycnoclines essentially envelop subsurface AW throughout the Nordic seas. Exchanges of heat, salt, and mass across both pycnoclines as well as exchanges of heat and freshwater across the air–sea surface combine to modify AW as it circulates the basin.

In this study, we present a conceptual model for a boundary current that is divided by a thermocline and a halocline. This model describes the transformation of an Atlantic inflow as a downstream modification of the boundary current in the along-boundary dimension. This approach builds upon the model of Wåhlin and Johnson (2009) by including a qualitative hydrography as seen in Fig. 2. Using this model, we address the following questions:

- What processes affect water mass transformation in a transition zone?
- How can exchanges across a halocline and a thermocline interact?
- What features determine the impact of freshwater input on water mass transports?

In section 2, we formulate the conceptual model. In section 3, we discuss the boundary current transformation for a reference case with parameter values based on the Nordic seas. In section 4, we explore the impact of the magnitude and distribution of freshwater input on volume transports of the different water masses, and we end with a discussion in section 5 and concluding remarks in section 6.

2. Model configuration

Water masses in the Nordic seas can be—and often are—classified into three general types: AW, which is relatively warm and saline; PW, which is fresher and less dense; and DW, which is cold and the densest of the three water masses. We use this classification of three water masses to develop a three-layer boundary current, separated by a thermocline and a halocline which wrap around the basin (Fig. 3a). These nearby pycnoclines reflect the convergence of the alpha and beta oceans in the Nordic seas. As the boundary current circulates the basin, surface fluxes of heat and freshwater and cross-pycnocline exchanges of heat, salt, and mass induce downstream water mass transformation (Fig. 3b). This transformation alters the hydrography of the boundary current and induces net transformation of AW to DW and PW, accounting for an outflow of all three water masses as observed in the East Greenland Current (Håvik et al. 2017). We will consider a boundary current in steady state, which allows us to reduce the system into one dimension: the along-boundary position x relative to the inflow of AW into the basin (Fig. 3a).

In this section, we present a set of equations that describe a three-layer boundary current and its water mass transformation. Based on first principles and parameterizations, we derive expressions for temperature, salinity, and volume transport of each layer, either as constants or as a function of the along-boundary position x.

a. Conservation laws interior

The model basin is divided into two regimes: a boundary region that hosts the boundary current and an interior basin that has zero mean flow (Fig. 3b). Following

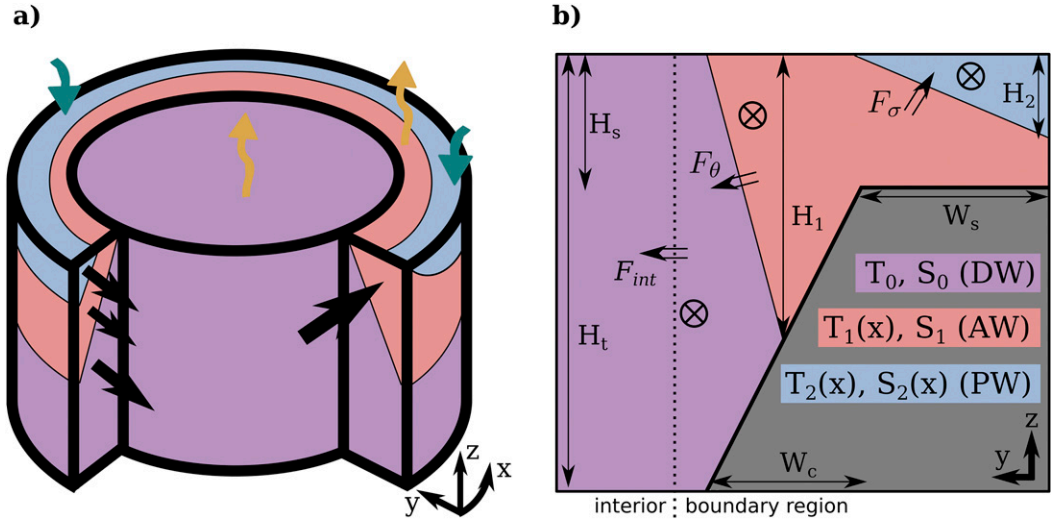

FIG. 3. Boundary current model. (a) Sketch of water mass distribution and surface fluxes. Arrows indicate inflows and outflows (black), surface heat loss (yellow), and runoff (blue). Variables x and y denote the along-boundary and cross-boundary distances, and z denotes the depth. (b) Detailed section across the boundary region and subsurface exchanges. The dashed line indicates the division between the motionless interior and the boundary region. Variable F indicates diffusive heat and salt fluxes across the thermocline θ and halocline σ and toward the interior F_{int}. Colors indicate the three water masses 0 (DW), 1 (AW), and 2 (PW). Layer thicknesses are denoted by H_1 (AW) and H_2 (PW). Bathymetry is defined by shelf depth H_s, interior depth H_t, continental slope width W_c, and continental shelf width W_s. Model dynamics are governed by five variables: DW temperature T_0, AW temperature T_1 and thickness H_1, and PW salinity S_2 and thickness H_2.

considerations of Spall (2004), we will assume this interior basin to be filled homogeneously with DW. This water mass will be referred to as layer 0.

Because the interior is motionless in steady state, no mean flow can occur between the interior and the boundary region. A steady-state heat budget in the interior can thus be written as

$$\int_0^L F_{\text{int}}^T \, dx = \iint_A Q_0 \, dx \, dy. \tag{1}$$

Here, F_{int}^T is the vertically integrated heat flux from the boundary region to the interior ($\mathrm{W\,m^{-1}}$; Fig. 3b), x is the along-boundary position (m; Fig. 3a), L is the total length of the boundary current (m), Q_0 is the surface heat loss from the interior ($\mathrm{W\,m^{-2}}$), and $\iint_A \ldots dx\,dy$ denotes integration over the interior sea surface.

We parameterize surface heat loss by a relaxation to a homogeneous atmospheric temperature T_a (Haney 1971):

$$Q_i = \Gamma(T_i - T_a). \tag{2}$$

Here, Q_i is the surface heat loss from layer i ($\mathrm{W\,m^{-2}}$), Γ is a constant relaxation rate ($\mathrm{W\,m^{-2}\,°C^{-1}}$), and T_i is the temperature of layer i (°C). Note that this parameterization is only valid if T_i is above the freezing point, which is ensured if T_a is equal to or above the freezing point.

We only consider freshwater input feeding the shelf regions, as this is critical in establishing and maintaining salinity stratification over the continental shelves (Fig. 3b). This marks an essential contrast with previous studies considering only direct precipitation into the basin interior (e.g., Spall 2012). We choose to represent freshwater input as a virtual salt flux; as a consequence, the total volume in the basin is conserved. This approximation is valid as long as deviations in salinity from a reference value are small compared to the reference salinity itself, or similarly, if surface freshwater fluxes are small compared to volume transports. Without any mean volume exchange between the boundary region and the interior, conservation of salt in the interior is given by

$$\int_0^L F_{\text{int}}^S \, dx = 0, \tag{3}$$

where F_{int}^S is the vertically integrated salt flux from the boundary region to the interior ($\mathrm{g\,kg^{-1}\,m^2\,s^{-1}}$; Fig. 3b).

b. Conservation laws boundary region

Using the Boussinesq approximation, we can transform mass conservation to volume conservation.

This can be expressed as a downstream conservation of volume transport:

$$\frac{d}{dx}(\Psi_0 + \Psi_1 + \Psi_2) = 0. \tag{4}$$

Here, Ψ_i is the along-boundary volume transport of layer i ($m^3 s^{-1}$), where $i = 1$ denotes AW and $i = 2$ denotes PW (see Fig. 3b). As Ψ_0 is not zero, DW is divided between a motionless fraction filling the interior and a moving fraction in the boundary region (Fig. 3).

Conservation of heat can be similarly expressed as a downstream conservation of heat transport. The sinks of heat are lateral heat loss to the interior and surface heat loss from the outcrop regions of the different layers. This allows for the expression for heat conservation:

$$C_p \frac{d}{dx}(\Psi_0 T_0 + \Psi_1 T_1 + \Psi_2 T_2) = -F^T_{\text{int}} - Q_1 W_1 - Q_2 W_2. \tag{5}$$

Here, W_i is the cross-boundary outcrop width of layer i (m), and C_p is the specific heat coefficient ($J m^{-3} °C^{-1}$). We assume that surface heat loss from DW occurs predominantly from the motionless interior and hence neglect the surface heat loss from the moving fraction of DW in the boundary region. As a result, surface heat loss from the boundary current occurs only from the outcrop of AW and PW.

Similarly, conservation of salt in the boundary region can be expressed as

$$\frac{d}{dx}(\Psi_0 S_0 + \Psi_1 S_1 + \Psi_2 S_2) = -F^S_{\text{int}} - R S_2. \tag{6}$$

Here, S_i is the salinity of layer i in ($g kg^{-1}$) and R is the runoff entering the perimeter per unit length along the boundary ($m^2 s^{-1}$). Note that runoff R only enters layer 2 (PW), which forms the surface waters over the shelves (see Fig. 3b). This runoff represents both actual river runoff and freshwater outflows from surrounding basins (such as the Baltic and the Arctic Ocean) feeding into the shelf areas.

In the following sections, we break these conservation laws down to separate equations of volume transport, temperature, and salinity for the different layers. For this, we present explicit exchanges across the thermocline and the halocline which govern the distribution of volume, heat, and salt within the boundary region.

c. Cross-pycnocline exchange

Within the boundary region, the three layers can exchange heat and salt across the pycnoclines. We assume that two drivers dominate this exchange: mesoscale eddies and vertical diffusion. For example, the heat exchange across the thermocline can be expressed as

$$F^T_\theta = C_p \int_\theta \overline{v'T'}\, dz + C_p \int_\theta \overline{w'T'}\, dy. \tag{7}$$

Here, F^T_θ is the total cross-thermocline heat flux ($W m^{-1}$) from layer 1 to layer 0. The first term on the right-hand side is the vertically integrated lateral eddy heat flux, and the second term is the laterally integrated vertical diffusion.

Both eddy fluxes and vertical diffusion can be parameterized in terms of the local hydrography in the boundary region. For lateral eddy fluxes, we adopt a parameterization based on baroclinic instability (Visbeck et al. 1996; Spall 2004):

$$\int_\theta \overline{v'T'}\, dz = \frac{c_\theta g \Delta\rho_\theta (T_1 - T_0) H_1^2}{2 f \rho_{\text{ref}} W_\theta}. \tag{8}$$

Here, c_θ is the nondimensional eddy coefficient for the thermocline, g is the gravitational acceleration ($m s^{-2}$), $\Delta\rho_\theta$ is the density contrast across the thermocline ($kg m^{-3}$), ρ_{ref} is a reference density ($kg m^{-3}$), W_θ is the width of the thermocline (m), and H_1 is the thickness of layer 1 (m).

For vertical diffusion, we introduce a parameterization based on a constant vertical diffusivity. Vertical diffusion is related to the layer thickness of the water mass above the pycnocline (e.g., Nilsson and Walin 2010). Because of the outcrop of the pycnoclines, layer thicknesses vary across the boundary. To account for this, we will parameterize vertical diffusion based on the mean layer thickness which is equal to $H_1/2$ for the thermocline. For example, the expression of vertical heat diffusion across the thermocline is then given by

$$\int_\theta \overline{w'T'}\, dy = \frac{2\kappa^v W_\theta (T_1 - T_0)}{H_1}, \tag{9}$$

where κ^v is the vertical diffusivity ($m^2 s^{-1}$).

The thermocline width W_θ can be deduced from topography (see Fig. 3b) and is given by

$$W_\theta = \frac{W_c (H_t - H_1)}{H_t - H_s}, \tag{10}$$

where W_c is the width of the continental slope (m), H_t is the depth of the interior (m), and H_s is the depth of the continental shelf (m).

These parameterizations lead to an expression for the cross-thermocline heat flux in terms of a total diffusive flux due to combined mesoscale eddies and vertical diffusion:

$$F_\theta^T = C_p \kappa_\theta (T_1 - T_0), \tag{11}$$

where κ_θ is a state-dependent effective diffusivity ($m^2 s^{-1}$), given by

$$\kappa_\theta = \frac{c_\theta g \Delta\rho_\theta H_1^2 (H_t - H_s)}{2 f \rho_{\text{ref}} W_c (H_t - H_1)} + \frac{2\kappa^v W_c (H_t - H_1)}{H_1 (H_t - H_s)}. \tag{12}$$

Similarly, the total cross-thermocline salt flux can be derived in terms of the same effective diffusivity:

$$F_\theta^S = \kappa_\theta (S_1 - S_0), \tag{13}$$

where F_θ^S is the total cross-thermocline salt flux ($g\,kg^{-1}\,m^2\,s^{-1}$).

Finally, the cross-halocline heat and salt fluxes can be similarly derived and expressed as

$$F_\sigma^T = C_p \kappa_\sigma (T_1 - T_2), \quad \text{and} \tag{14a}$$

$$F_\sigma^S = \kappa_\sigma (S_1 - S_2). \tag{14b}$$

Here, κ_σ is the state-dependent effective diffusivity for the halocline ($m^2 s^{-1}$), given by

$$\kappa_\sigma = \frac{c_\sigma g \Delta\rho_\sigma H_2^2}{2 f \rho_{\text{ref}} W_s} + \frac{2\kappa^v W_s}{H_2}, \tag{15}$$

where c_σ is the nondimensional eddy coefficient for the halocline; $\Delta\rho_\sigma$ is the density contrast across the halocline ($kg\,m^{-3}$); W_s is the width of the continental shelf (m), equal to the width of the halocline; and H_2 is the thickness of layer 2 (m).

d. Water mass transformation

The cross-pycnocline fluxes extract heat and salt from the Atlantic layer and induce an along-boundary water mass transformation. Previous idealized studies have represented this water mass transformation in two qualitative ways. Spall (2012) considered conservation of AW volume transport, resolving the downstream extraction of heat and salt by a gradual cooling and freshening of AW. Straneo (2006) considered conservation of AW hydrography, resolving the downstream extraction of heat and salt by a transformation of a fraction of AW to DW. (Note that the latter model was formulated in terms of buoyancy rather than temperature and/or salinity.)

What processes drive the transformation of AW to DW and PW in the Nordic seas is not fully understood, and we will not attempt to resolve this issue in the current study. Instead, we introduce a closure that follows Straneo (2006), in which all cross-thermocline exchange induces a qualitative transformation of AW to DW. Similarly, all cross-halocline exchange induces a transformation of AW to PW. This closure is illustrated in Fig. 4 and applies when abundant mixing optimally distributes exchanged heat and salt throughout layer 0 (e.g., by deep convection) and layer 2 (e.g., by wind stress). Note that the important constraints of heat and salt conservation do not depend on this closure and that the cross-pycnocline exchange of heat and salt are governed by the parameterized processes as formulated above.

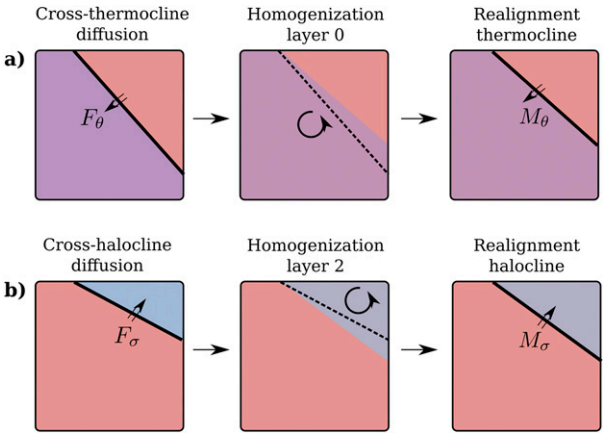

FIG. 4. Relation between cross-pycnocline diffusion and transformation of AW. (a) Diffusion across the thermocline F_θ induces transformation of AW to DW M_θ, decreasing AW transport Ψ_1 by decreasing AW thickness H_1. (b) Diffusion across the halocline F_σ induces transformation of AW to PW M_σ, increasing PW transport Ψ_2 by increasing its thickness H_2. Note that both DW and PW warm and salinify due to these diffusive processes, whereas AW hydrography is unperturbed by diffusion.

If all extraction of heat and salt from AW across the thermocline induces a transformation of a fraction of AW to DW, this closure can be formulated as

$$F_\theta^T = C_p M_\theta (T_1 - T_0). \tag{16}$$

Here M_θ is the transformation rate of AW to DW ($m^2 s^{-1}$). Note that this closure requires an equivalent relation for the exchange of salt, which is implicit due to the expression of cross-pycnocline exchanges in terms of a total diffusive flux.

The relation between the cross-thermocline heat and salt fluxes and the transformation of AW to DW can be summarized by the relation

$$M_\theta = \kappa_\theta. \tag{17}$$

The along-boundary transformation rate of AW to DW is thus determined by the effective cross-thermocline diffusivity. Similarly, the relation between the cross-halocline heat and salt fluxes and the transformation of AW to PW can be expressed as

$$M_\sigma = \kappa_\sigma, \tag{18}$$

where M_σ is the transformation rate of AW to PW ($m^2 s^{-1}$).

The transformation rates represent cross-pycnocline volume fluxes, reducing the volume transport of AW downstream and increasing the volume transport of DW and PW. Conservation of volume in each layer can thus be expressed as

$$\frac{d\Psi_0}{dx} = M_\theta, \tag{19a}$$

$$\frac{d\Psi_1}{dx} = -M_\theta - M_\sigma, \quad \text{and} \tag{19b}$$

$$\frac{d\Psi_2}{dx} = M_\sigma. \tag{19c}$$

As illustrated in Fig. 4, the total heat transport across the pycnoclines is equal to the heat carried by transformed AW. This transport includes the diffusive heat flux as well as the heat carried by the enhanced volume transport of DW and PW. Conservation of heat in each layer is then given by

$$C_p \frac{d\Psi_0 T_0}{dx} = -F^T_{\text{int}} + C_p M_\theta T_1, \tag{20a}$$

$$C_p \frac{d\Psi_1 T_1}{dx} = -C_p M_\theta T_1 - C_p M_\sigma T_1 - Q_1 W_1, \quad \text{and} \tag{20b}$$

$$C_p \frac{d\Psi_2 T_2}{dx} = C_p M_\sigma T_1 - Q_2 W_2. \tag{20c}$$

Similarly, conservation of salt in each layer is given by

$$\frac{d\Psi_0 S_0}{dx} = -F^S_{\text{int}} + M_\theta S_1, \tag{21a}$$

$$\frac{d\Psi_1 S_1}{dx} = -M_\theta S_1 - M_\sigma S_1, \quad \text{and} \tag{21b}$$

$$\frac{d\Psi_2 S_2}{dx} = M_\sigma S_1 - R S_2. \tag{21c}$$

e. Hydrographic transformation

From the above layer-by-layer conservation laws, we can derive expressions for the downstream changes in hydrography:

$$C_p \Psi_0 \frac{dT_0}{dx} = -F^T_{\text{int}} + F^T_\theta, \tag{22a}$$

$$C_p \Psi_1 \frac{dT_1}{dx} = -Q_1 W_1, \tag{22b}$$

$$C_p \Psi_2 \frac{dT_2}{dx} = F^T_\sigma - Q_2 W_2, \tag{22c}$$

$$\Psi_0 \frac{dS_0}{dx} = -F^S_{\text{int}} + F^S_\theta, \tag{22d}$$

$$\Psi_1 \frac{dS_1}{dx} = 0, \quad \text{and} \tag{22e}$$

$$\Psi_2 \frac{dS_2}{dx} = F^S_\sigma - R S_2. \tag{22f}$$

Note that because of the direct relation between transformation rates and cross-pycnocline exchange of heat and salt, AW hydrography is only perturbed by direct surface fluxes.

To retain homogeneity in layer 0, both in the interior and in the moving fraction in the boundary region, we assume $F^T_{\text{int}} = F^T_\theta$ and $F^S_{\text{int}} = F^S_\theta$, so that

$$\frac{dT_0}{dx} = \frac{dS_0}{dx} = 0. \tag{23}$$

As both S_1 and S_0 are invariant along the boundary, and M_θ is nonzero, Eq. (3) can only be satisfied if $S_0 = S_1$. This is a direct consequence of the absence of surface freshwater input into the interior, in contrast to the model presented by Spall (2012). Further, the fact that both S_1 and S_0 are invariant along the boundary implies that all freshwater is retained within layer 2 and exported by PW. This implies that the model does not resolve any freshwater leakage off the shelves.

Altogether, three hydrographic properties vary downstream: AW temperature T_1, PW temperature T_2, and PW salinity S_2. Additionally, the volume transports of each layer vary due to net transformation of AW to DW and PW.

f. Volume transport

To express the volume transport of each layer, we introduce an idealized velocity structure to approximate the reanalysis fields in Fig. 2. The velocity structure is marked by two baroclinic currents, one associated with the thermocline and one with the halocline. In addition, we assume that the along-boundary transport of AW and PW is restricted to the water above these pycnoclines. This is in general agreement with the reanalysis fields, where along-boundary velocities below the thermocline and the halocline are small. Finally, and most importantly, we assume that the along-boundary velocity maintains thermal wind balance at each point along the boundary.

Based on these assumptions, one baroclinic current aligns over the continental shelf (see Fig. 3b). The transport of PW is restricted above the halocline by

assuming a level of no motion at the depth of the halocline and that the underlying AW is motionless. The volume transport of such a baroclinic current, which is equal to the volume transport of PW, was derived by Werenskiold (1935):

$$\Psi_2 = \frac{g\Delta\rho_\sigma H_2^2}{2f\rho_{\text{ref}}}. \tag{24}$$

The second baroclinic current aligns over the continental slope. We assume a similar velocity structure which is constrained by a level of no motion at the depth of the thermocline. Further, we assume that the underlying DW below the thermocline is motionless, leading to an equivalent expression for AW transport:

$$\Psi_1 = \frac{g\Delta\rho_\theta H_1^2}{2f\rho_{\text{ref}}}. \tag{25}$$

Note that with these expressions, the lateral eddy fluxes across the halocline [Eq. (15)] scale linearly with PW transport [Eq. (24)], and the lateral eddy fluxes across the thermocline [Eq. (12)] scale linearly with AW transport [Eq. (25)].

Finally, we assume that the transport of DW is not directly related to hydrography. This is achieved by restricting the transport of DW to a narrow barotropic current directly offshore from the continental slope. This narrow current is considered part of the boundary region (see Fig. 3b). As the velocity of this current is not related to hydrography through thermal wind balance, the along-boundary volume transport of DW follows from volume conservation.

Note that this velocity structure is idealized, and we do not explicitly resolve the associated vertical and cross-boundary velocities. Further, note that this velocity structure differs from that in comparable, idealized models. In the model by Straneo (2006), a barotropic current aligns over the continental slope; and in the model by Walin et al. (2004), a barotropic current aligns over the continental shelves.

g. Equation of state

The density of the different water masses is given by the equation of state. Ignoring any pressure-related terms, the density contrasts across the pycnoclines are a function of the temperatures and the salinities of the different water masses. We will assume a linear equation of state which describes a density contrast across the thermocline given by

$$\Delta\rho_\theta = \rho_{\text{ref}}\alpha(T_1 - T_0). \tag{26}$$

Here, α is the thermal expansion coefficient ($^\circ\text{C}^{-1}$). Because no direct freshwater input feeds into the interior, salinities S_1 and S_0 are equal. As a result, the model generally overestimates the density contrast with respect to the Nordic seas (where $S_0 < S_1$; see Fig. 2). The lack of a salinity contrast across the thermocline also prevents any qualitatively different circulation states as found by Spall (2012).

For the density contrast across the halocline, we assume $\alpha(T_1 - T_2) \ll \beta(S_1 - S_2)$, leading to an equivalent equation of state governed by salinity:

$$\Delta\rho_\sigma = \rho_{\text{ref}}\beta(S_1 - S_2). \tag{27}$$

Here, β is the haline contraction coefficient [$(\text{g kg}^{-1})^{-1}$]. This approximation introduces a similar overestimation of the density contrast with respect to the Nordic seas, as PW is typically colder than AW. As both equations of state are determined by a single hydrographic tracer, they define an optimal distinction between the alpha and beta oceans within the boundary current.

h. Summary

The equations presented in this section describe a model for the dynamics and water mass transformation of the boundary current. Because the temperature contrast across the halocline is neglected in the density contrast [Eq. (27)], T_2 adopts a merely diagnostic role without impacting any other variable. We therefore omit dT_2/dx from the model equations, leaving a set of five equations which govern the boundary current's dynamics:

$$\frac{dS_2}{dx} = \frac{2f\kappa_\sigma}{g\beta H_2^2} - \frac{2fRS_2}{g\beta(S_1 - S_2)H_2^2}, \tag{28a}$$

$$\frac{dH_2}{dx} = \frac{2f\kappa_\sigma}{g\beta(S_1 - S_2)H_2} - \frac{fRS_2}{g\beta(S_1 - S_2)^2 H_2}, \tag{28b}$$

$$\frac{dT_1}{dx} = -\frac{2f\Gamma W_c(T_1 - T_a)}{C_p g\alpha(T_1 - T_0)H_1^2}, \tag{28c}$$

$$\frac{dH_1}{dx} = -\frac{f\kappa_\theta}{g\alpha(T_1 - T_0)H_1} - \frac{f\kappa_\sigma}{g\alpha(T_1 - T_0)H_1} + \frac{\Gamma W_c f(T_1 - T_a)}{C_p g\alpha(T_1 - T_0)^2 H_1}, \quad \text{and} \tag{28d}$$

$$T_0 = T_a + \frac{C_p}{\Gamma A}\int_0^L \kappa_\theta(T_1 - T_0)\,dx. \tag{28e}$$

These equations are closed by the following expressions for the effective diffusivities across both pycnoclines:

TABLE 1. Model parameters.

Physical description	Symbol	Reference value	Units	Reference
Inflow AW temperature	$T_1(0)$	8	°C	Eldevik and Nilsen (2013)
Inflow AW salinity	$S_1(0)$	35.2	$g\,kg^{-1}$	Eldevik and Nilsen (2013)
Inflow AW thickness	$H_1(0)$	600	m	Eldevik and Nilsen (2013)
Inflow PW salinity	$S_2(0)$	35.1	$g\,kg^{-1}$	Chosen to give small PW inflow transport
Inflow PW thickness	$H_2(0)$	10	m	Chosen to give small PW inflow transport
Inflow DW transport	$\Psi_0(0)$	0	$m^3\,s^{-1}$	
Depth shelves	H_s	200	m	
Depth interior	H_t	1000	m	
Width shelves	W_s	100	km	
Width slope	W_c	100	km	
Interior surface area	A	1.5×10^6	km^2	
Length boundary	L	5.0×10^3	km	
Thermal expansion coefficient	α	1.0×10^{-4}	$°C^{-1}$	Based on $T = 4°C$
Haline contraction coefficient	β	8×10^{-4}	$(g\,kg^{-1})^{-1}$	
Gravitational acceleration	g	9.8	$m\,s^{-2}$	
Coriolis parameter	f	1.4×10^{-4}	s^{-1}	Based on 75°N
Volumetric heat capacity	C_p	4.2×10^6	$J\,m^{-3}\,°C^{-1}$	
Eddy coefficient thermocline	c_θ	0.007		Spall (2012)
Eddy coefficient halocline	c_σ	0.025		Visbeck et al. (1996); Spall (2013)
Vertical diffusivity	κ^v	1×10^{-4}	$m^2\,s^{-1}$	
Atmospheric temperature	T_a	−2	°C	Chosen to give reasonable AW inflow transport
Restoring strength	Γ	20	$W\,m^{-2}\,°C^{-1}$	Ill constrained, see discussion by Wåhlin and Johnson (2009)
Runoff	R	0.02	$m^2\,s^{-1}$	

$$\kappa_\theta = \frac{c_\theta g\alpha(T_1 - T_0)H_1^2(H_t - H_s)}{2fW_c(H_t - H_1)} + \frac{2\kappa^v W_c(H_t - H_1)}{H_1(H_t - H_s)},$$

and (29a)

$$\kappa_\sigma = \frac{c_\sigma g\beta(S_1 - S_2)H_2^2}{2fW_s} + \frac{2\kappa^v W_s}{H_2}. \quad (29b)$$

The right-hand-side terms of Eq. (28) represent the four processes that govern the downstream water mass transformation of the boundary current: cross-thermocline diffusion (terms including κ_θ), cross-halocline diffusion κ_σ, surface heat loss from layer 1 ΓW_c, and runoff R. In the following section, we discuss, based on a reference case for constant parameters, how these four processes affect the five unknowns of Eq. (28) and shape the boundary current.

3. Reference case

The model described by Eq. (28) consists of five unknowns: PW salinity S_2 and thickness H_2, AW temperature T_1 and thickness H_1, and DW temperature T_0. As a reference case, we choose a list of parameters that reasonably describe the circulation in the Nordic seas (Table 1). As atmospheric temperature T_a we choose a value equal to freezing temperature to ensure that freezing processes can be neglected. Equation (28) is solved through an iterative process starting with an initial guess for T_0, integrating Eqs. (28a)–(28d), solving Eq. (28e), and adjusting the initial guess of T_0 accordingly. This process leads to a unique solution for the five unknowns in Eq. (28), which is shown in Fig. 5. Throughout the remainder of this section, we will keep all parameters constant as we explore how the model resolves the circulation of AW and its transformation to DW and PW.

For this reference case, we observe a downstream cooling of AW. The modification of PW is characterized by a freshening throughout the first 2000 km and a salinification further downstream. Finally, the thickness of AW decreases slightly, whereas the thickness of PW increases significantly. This transformation of PW agrees qualitatively with the reanalysis sections across the eastern Nordic seas (Fig. 2). Across section B, a fresh, shallow layer is observed over the continental shelf; further downstream, across section C, this layer is more saline and extends deeper.

From the reference solutions, we derive a number of diagnostics which help understand the model dynamics (Fig. 6). The first diagnostics are the volume transports of the three water masses (see Fig. 6a). As determined by boundary conditions, all inflow ($x = 0$) consists of AW. As the boundary current circulates the basin, this

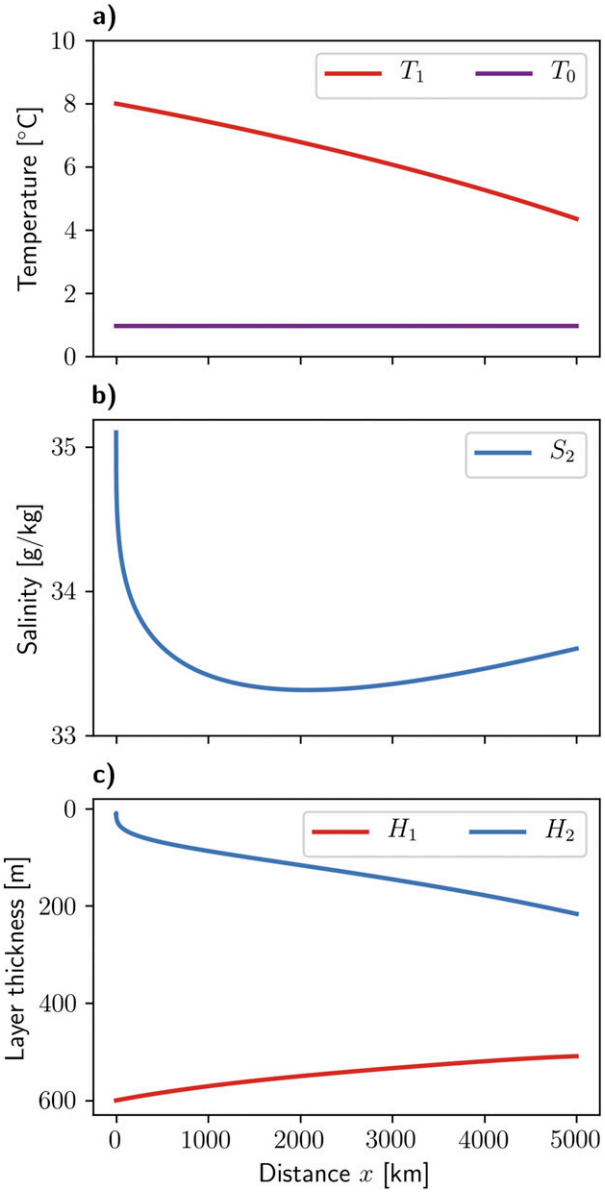

FIG. 5. Evolution of boundary current variables. (a) Temperature of AW T_1 and DW T_0. (b) Salinity of PW S_2. (c) Layer thickness of AW H_1 and PW H_2. Solutions for the five variables governing the boundary current as described in Eq. (28). Solutions are based on parameters listed in Table 1.

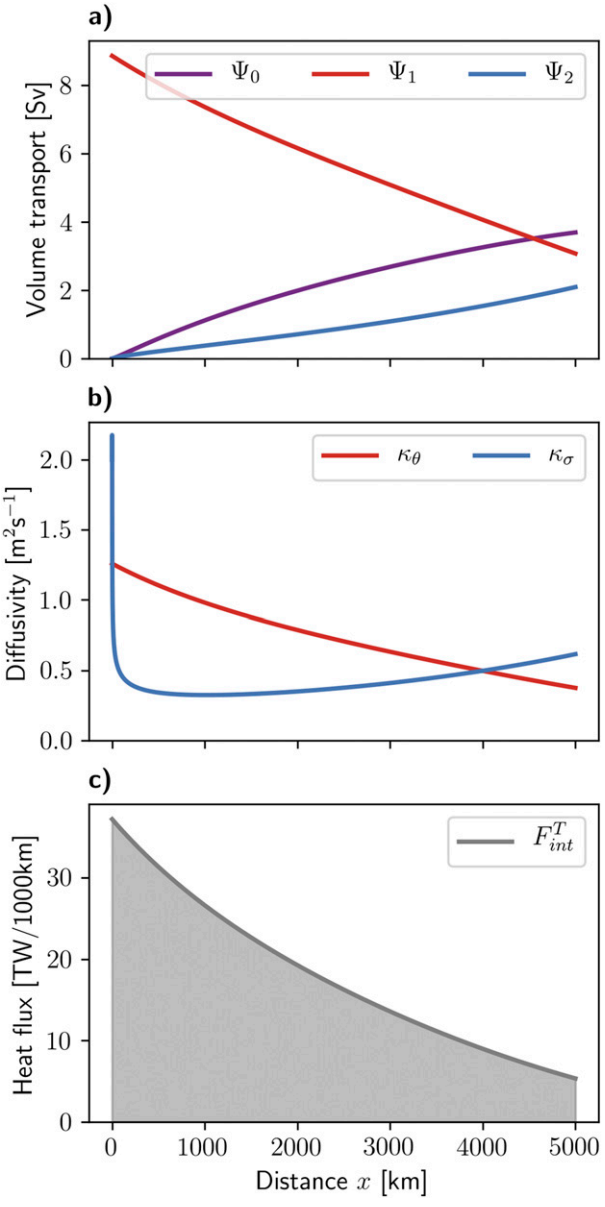

FIG. 6. Evolution of main boundary current diagnostics. (a) Volume transports of DW Ψ_0, AW Ψ_1, and PW Ψ_2. (b) Effective diffusivities across the thermocline κ_θ and the halocline κ_σ governing the transformation from AW to DW and PW, respectively. (c) Lateral heat flux from the boundary region to the interior. Total heat flux toward the interior is indicated by the integral (gray shading).

AW is transformed partly into DW, and partly into PW. These transformations are governed by cross-pycnocline exchanges, quantified in terms of effective diffusivities [Eq. (29); Fig. 6b]. The cross-thermocline exchange decreases along the boundary, indicating that the production of DW is dominant near the inflow. The cross-halocline exchange shows a peak just downstream from the inflow and increases monotonically beyond 1000 km. This indicates that significant production of PW is near the outflow, and beyond 4000 km, more AW is transformed to PW than to DW. The last diagnostic which is crucial to understanding model behavior describes the interaction between the boundary region and the interior: the lateral heat flux (Fig. 6c). As this heat flux is directly linked to DW production, it also decreases monotonically around the basin.

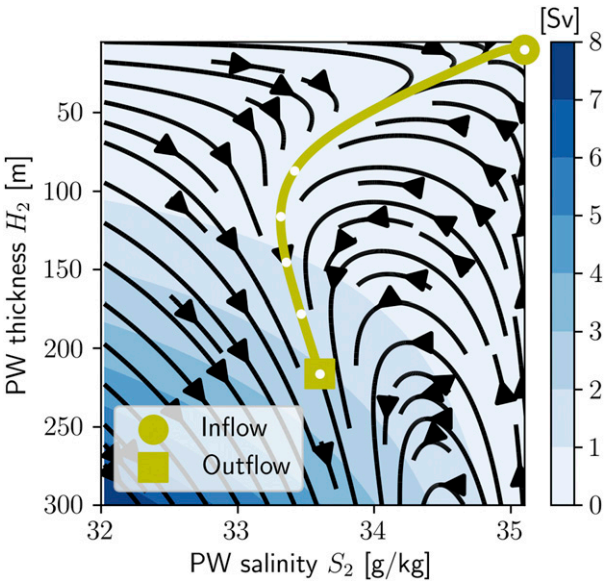

FIG. 7. Transformation field of PW. The arrows indicate the downstream tendencies dH_2/dx and dS_2/dx. The shading indicates PW volume transport Ψ_2. The yellow line projects the reference solutions of H_2 and S_2 (Figs. 5b,c). White dots indicate the distance along the boundary with intervals of 1000 km.

In the remainder of this section, we will explain how the solutions for the reference case arise from the four different water mass transformation processes described at the end of section 2. These four processes are cross-thermocline diffusion, cross-halocline diffusion, surface heat loss from AW, and runoff. We will discuss the impact of these processes on the individual water masses, proceeding from PW (described by S_2 and H_2) through AW (T_1 and H_1) to DW (T_0).

a. Polar Water properties

The transformation of PW properties is described by Eqs. (28a) and (28b). It is important to notice that these equations are only dependent on the two variables (S_2 and H_2) describing PW itself (note that κ_σ is only a function of S_2 and H_2 as well). In this model, the downstream evolution of PW can therefore be described as a separate system which is independent of the other three unknowns describing AW and DW properties.

As PW is described as a separate system of two equations and two unknowns, the downstream tendencies dS_2/dx and dH_2/dx are uniquely defined for each value of S_2 and H_2. Hence, we can visualize Eqs. (28a) and (28b) as a transformation field (Fig. 7), which is equivalent to a phase space diagram, commonly used in dynamical systems analysis. This transformation field functions as a road map for the downstream evolution of PW, which is then defined by the boundary conditions at inflow and the boundary length. From the converging nature of the transformation field, we can derive that small changes in inflow boundary conditions would have a small effect on the evolution of PW. In contrast, changes in boundary length would modify the outflow properties of PW by allowing for more or less water mass transformation along the centerline in this transformation field.

To better understand the underlying processes of PW transformation, we can extract the contributions of the individual processes: cross-halocline diffusion and runoff (Fig. 8). These fields visualize the separate terms on the right-hand side of Eqs. (28a) and (28b). Cross-halocline diffusion acts to increase the thickness, salinity, and volume transport of PW. Runoff acts to decrease both the thickness and salinity of PW along lines of constant volume transport. From these, we see that cross-halocline diffusion dominates the transformation of PW thickness H_2, which increases along the full basin. The transformation of PW salinity S_2 is dominated by runoff throughout the first 2000 km where freshening occurs. Farther downstream, the salinification of PW, which is also present in the reanalysis fields (Fig. 2), can be attributed to cross-halocline diffusion. Along with a salinification, this process induces an increase in the volume transport of PW.

It is insightful to consider the relative contribution of eddy fluxes and vertical diffusion to the total cross-halocline exchange (Fig. 9). Throughout the first 2000 km, vertical diffusion dominates due to the relatively shallow halocline. However, as the volume transport of PW increases downstream, the baroclinic shear across the halocline increases and eddy fluxes become more dominant. In particular near the outflow, where PW formation is strong, the bulk of cross-halocline exchange is governed by eddy fluxes. From this diagram, we can conclude that vertical diffusion primarily functions to deepen the halocline, which then strengthens eddy-induced exchange.

b. Atlantic Water properties

The transformation of AW properties (T_1 and H_1) is described by Eqs. (28c) and (28d). This transformation is more complex than that of PW, as it depends on κ_σ and T_0. It is therefore only possible to draw a unique transformation field of AW in terms of T_1 and H_1 for constant values of κ_σ, which in practice varies along the boundary (Fig. 6b).

To illustrate the transformation of AW and the impact of PW production on this transformation, we consider two constant values of κ_σ. The first, $\kappa_\sigma = 0\,\mathrm{m^2\,s^{-1}}$, represents the system without PW; this is essentially a two-layer system of AW and DW which can be directly

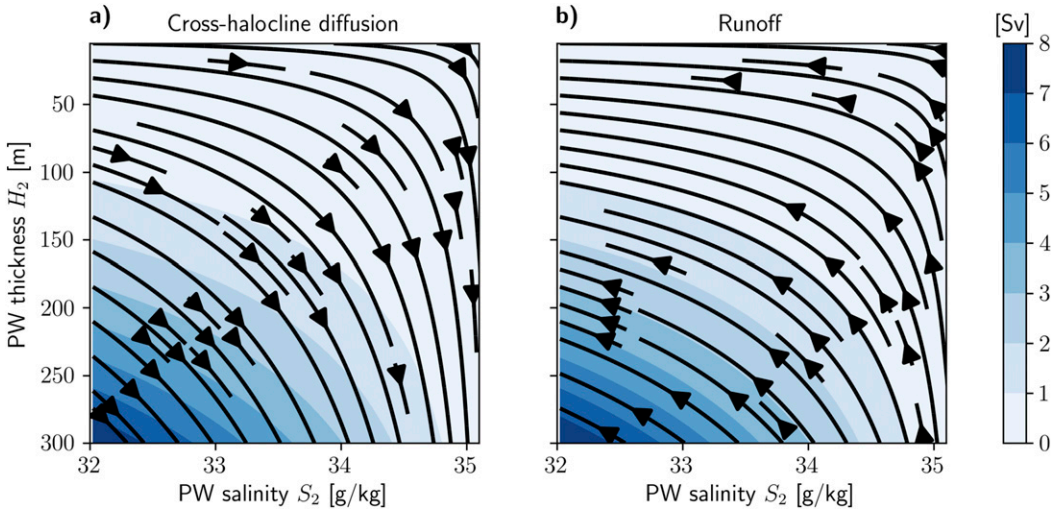

FIG. 8. Transformation of PW due to isolated processes. The arrows indicate the combined downstream tendencies dH_2/dx and dS_2/dx due to (a) cross-halocline diffusion and (b) runoff. The shading indicates PW volume transport Ψ_2.

compared to other boundary-current models without runoff and without salinity stratification in the boundary current (e.g., Spall 2012; Walin et al. 2004; Straneo 2006). The transformation field associated with this system is shown in Fig. 10a. In this transformation field, AW temperature T_1 converges to the same value of T_0. AW thickness converges to approximately 600 m if T_1 is relatively warm and increases if T_1 is relatively cold.

The second value for κ_σ (Fig. 10b) is $0.4\,\mathrm{m^2\,s^{-1}}$ is equal to the average value in the reference case. This represents a constant effective diffusivity across the halocline and consequently a constant transformation rate of AW to PW which amounts to 2 Sv along the complete boundary. Compared to the system without PW formation, we see a stronger tendency to reduce the AW thickness. Further, the outflow temperature of T_1 and the interior temperature T_0 are slightly decreased.

This impact can be understood from looking at the transformation due to the separate processes that affect AW properties (Fig. 11). As a result of the closure between cross-pycnocline exchange and the transformation of AW to DW and PW, these processes only act to reduce AW thickness along lines of constant AW temperature. Surface heat loss acts to reduce AW temperature and increase AW thickness along lines of constant volume transport. The convergence of AW thickness in Fig. 10 for relatively warm AW is thus a balance between cross-pycnocline exchange and surface heat loss. As no processes increase AW temperature or volume transport, these necessarily decrease along the complete boundary.

We can again separate the relative impact of eddy fluxes and vertical diffusion to the cross-thermocline exchange (Fig. 12). This indicates that vertical diffusion across the thermocline is small due to the relatively deep extent of the thermocline. This is in agreement with a priori assumptions in comparable studies which neglect vertical diffusion across the thermocline (Spall 2004; Straneo 2006).

Altogether, the transformation of AW properties can be summarized by a net cooling and a reduction of its volume transport. The production of PW through cross-halocline exchange enhances the reduction of AW thickness and

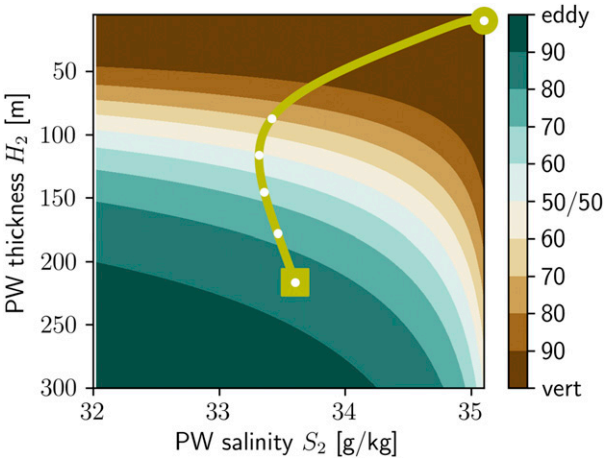

FIG. 9. Relative contributions to cross-halocline diffusion. Shading indicates the percentage of eddy and vertical diffusion to the total cross-halocline diffusion in Fig. 8a. The yellow line projects the reference solutions of H_2 and S_2 (Figs. 5b,c). White dots indicate the distance along the boundary with intervals of 1000 km.

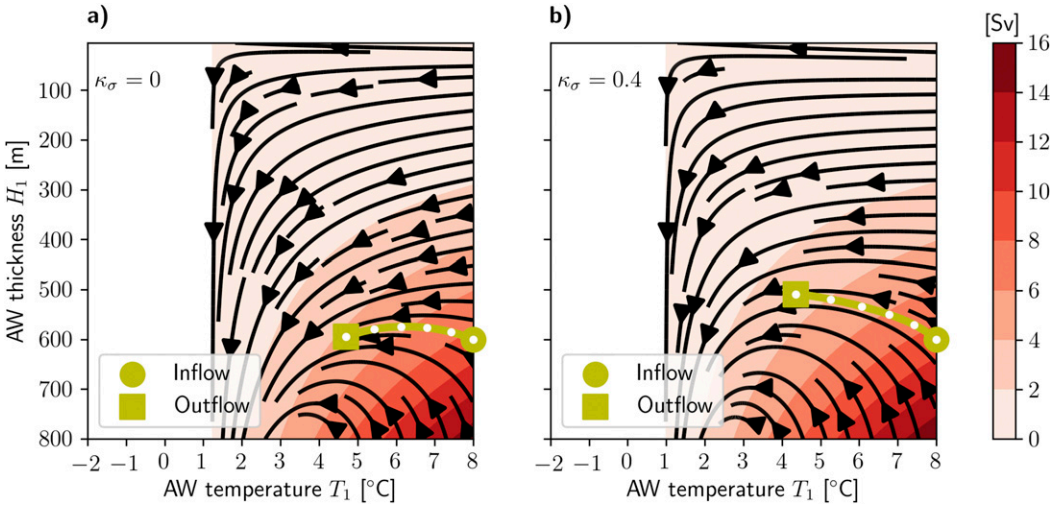

FIG. 10. Transformation field of AW. The arrows indicate the downstream tendencies dH_1/dx and dT_1/dx for constant values of κ_σ. (a) Transformation field without cross-halocline diffusion ($\kappa_\sigma = 0\,\mathrm{m^2\,s^{-1}}$). The shading indicates AW volume transport Ψ_1. The yellow line projects the solution obtained in absence of runoff and PW formation. (b) Transformation field based on average cross-halocline diffusivity ($\kappa_\sigma = 0.4\,\mathrm{m^2\,s^{-1}}$). The yellow line indicates the actual solution for the reference case (Figs. 5a,c). White dots indicate the distance along the boundary with intervals of 1000 km.

transport. Indirectly, this process enhances the cooling of AW temperature.

c. Deep Water temperature

The last of the five unknowns determining the boundary current is DW temperature T_0. As DW is homogeneous, T_0 has a single value throughout the basin. DW temperature is determined by a balance between lateral heat fluxes from the boundary region to the interior and surface heat fluxes from the interior sea surface to the atmosphere [Eq. (1)].

Lateral heat fluxes from the boundary region to the interior are equal to the diffusive heat fluxes across the thermocline which are dominated by eddies (Fig. 12). The lateral heat flux is thus closely related to the baroclinic instability of the slope current which governs eddy heat fluxes. Because of the transformation of AW to both DW and PW, the volume transport of the slope current that carries AW decreases downstream (Fig. 6a). This stabilizes the slope current and suppresses eddy diffusion downstream, which is reflected by the downstream weakening of lateral heat fluxes (Fig. 6c). The bulk of the heat flux determining T_0 is thus accounted for by lateral heat loss in the first half of the boundary current.

The temperature of DW plays a crucial role in the volume budget. As the volume transport at $x = 0$ consists of

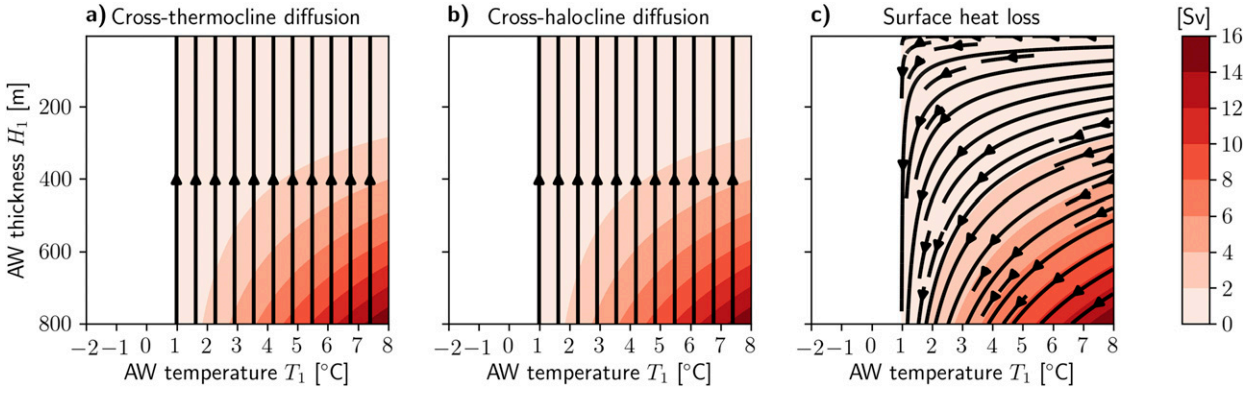

FIG. 11. Transformation of AW due to isolated processes. The arrows indicate the combined downstream tendencies dH_1/dx and dT_1/dx due to (a) cross-thermocline diffusion, (b) cross-halocline diffusion, and (c) surface heat loss from AW outcrop. Shading indicates AW volume transport Ψ_1. Note that no solutions are shown for $T_1 < T_0$.

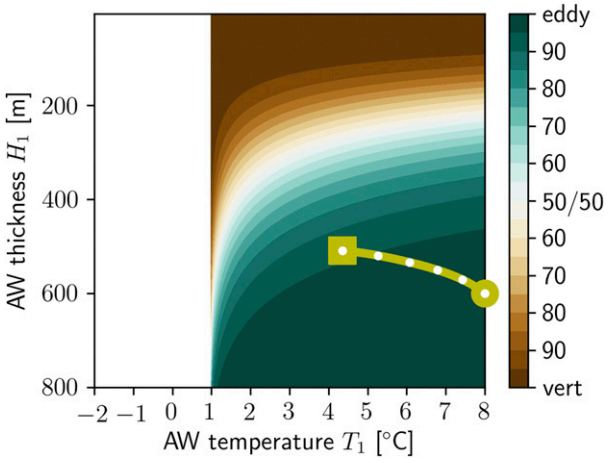

FIG. 12. Relative contributions to cross-thermocline diffusion. Shading indicates the percentage of eddy and vertical diffusion to the total cross-thermocline diffusion in Fig. 11a. The yellow line projects reference solutions of H_1 and T_1 (Figs. 5a,c). White dots indicate the distance along the boundary with intervals of 1000 km.

only AW, and boundary conditions $T_1(0)$ and $H_1(0)$ are given parameters, T_0 is the only variable that directly impacts the inflow transport of AW. A cold interior (low T_0) gives a strong temperature contrast across the thermocline where AW enters the basin, leading to a strong inflow transport.

4. Runoff impact

Runoff maintains a salinity stratification over the continental shelves and is an essential ingredient for PW formation in the model. In this section, we will analyze the impact of variations in runoff R by diagnosing the volume transports of the different water masses. In particular, we are interested in the strength of the Atlantic inflow and the outflows of DW and PW. We start with discussing uniform runoff of different magnitude; later in the section, we discuss the impact of runoff distribution along the boundary.

The impact of runoff magnitude on the different volume transports is shown in Fig. 13. For each value of runoff, AW transport decreases downstream, and both DW and PW transports increase. Runoff most strongly impacts the production of PW, which strengthens with increased runoff. This can be understood from the balance between runoff and eddy diffusion, which governs the bulk of PW formation. More runoff leads to a stronger increase in the salinity contrast across the halocline downstream, and consequently increases the baroclinic instability of the coastal current. As diffusion directly induces a transformation of AW to PW in the model, more runoff leads to an enhanced reduction of AW transport (as seen in Fig. 10). This enhanced reduction in AW transport in turn reduces the baroclinic instability of the slope current and suppresses DW production which is limited for relatively large values of runoff.

These direct and indirect effects of runoff raise the question whether different runoff sources impact the system differently. To study the impact of runoff distribution, we divide runoff R into three sources, motivated by the freshwater inflows into the Nordic seas (Fig. 14). A uniform background runoff of 20 mSv represents the river runoff from the Norwegian and Greenland coasts, a freshwater pulse nearby the Atlantic inflow represents the Baltic freshwater outflow, and a freshwater pulse farther downstream represents the Arctic freshwater outflow.

The impact of variations in the Arctic and Baltic freshwater outflows is quantified by the inflow of AW and the outflows of DW and PW (Fig. 15). Qualitatively, these volume transports respond similarly to changed freshwater input from the two sources. Enhanced freshwater input increases the total production of PW and decreases the total production of DW, which is in agreement with

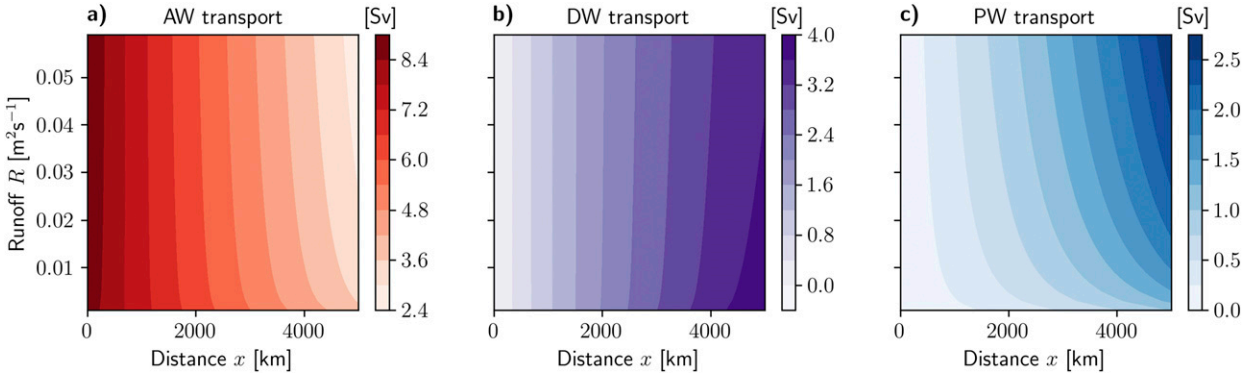

FIG. 13. Downstream evolution of volume transports as a function of uniform runoff. (a) AW transport Ψ_1, (b) DW transport Ψ_0, and (c) PW transport Ψ_2. Solutions for $R = 0.02\,\mathrm{m^2\,s^{-1}}$ are equal to the reference case shown (Fig. 6a).

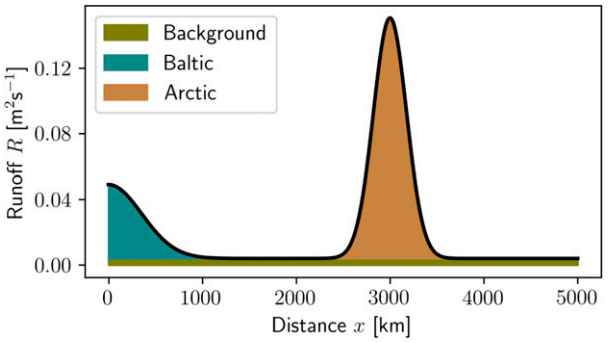

FIG. 14. Position-dependent runoff. Model input $R(x)$ used to simulate three freshwater sources. In this example, freshwater flux of background runoff equals 20 mSv, Baltic outflow equals 20 mSv, and Arctic outflow equals 65 mSv, which are equal to present-day observations.

increased uniform runoff (Fig. 13). Increased freshwater input also strengthens the AW inflow, albeit slightly.

The relative impacts of freshwater that enters from the Baltic and from the Arctic differ greatly. With respect to present-day freshwater input (20 mSv from the Baltic, 65 mSv from the Arctic as marked in Fig. 15), the sensitivity of total PW production to changes in the Baltic freshwater outflow is a factor of 9 greater than the sensitivity to changes in the Arctic freshwater outflow. This implies that a 1-mSv increase in Baltic freshwater outflow to the Nordic seas would have the same effect on PW outflow as a 9-mSv increase in Arctic freshwater outflow. In relative terms, a 10% increase in Baltic freshwater outflow would have the same effect as a 28% increase in Arctic freshwater outflow. The simple explanation for this difference in sensitivities is that freshwater entering the marginal sea farther upstream has a longer pathway where it can impact the estuarine circulation.

An even larger difference in sensitivities is found for DW outflow (a factor of 18) and AW inflow (a factor of 28). The processes that induce DW formation and the lateral heat fluxes to the interior dominate in the first half of the boundary region. Most of this transformation occurs upstream from the location where the Arctic freshwater outflow enters the basin. This greatly suppresses the potential for Arctic freshwater to impact water mass transformation related to DW formation and heat fluxes to the interior and hence the AW inflow which is determined by these heat fluxes. Baltic freshwater, on the other hand, enters the basin upstream from the region where active water mass transformation occurs. This greatly enhances the potential impact of Baltic freshwater on the basinwide circulation.

5. Discussion

The model presented in this paper builds upon a number of previous idealized studies that have addressed circulation and water mass transformation of AW in a marginal sea due to surface heat loss and freshwater input. Some of these studies have prescribed the volume transport of inflowing AW (e.g., Wåhlin and Johnson 2009; Straneo 2006), whereas others have attempted to resolve the sensitivity of the circulation strength to either the large-scale wind field (e.g., Nøst and Isachsen 2003) or the water mass transformation within the marginal sea (e.g., Spall 2004; Walin et al. 2004; Spall 2012). The approach of the present study most closely follows the latter, as we have tried to illustrate the potential impact of coastal freshwater sources on the circulation strength. We find a qualitatively similar freshwater sensitivity to that found in a box model by Lambert et al. (2016), as coastal freshwater input into buoyant surface waters can increase the overall circulation strength. However, these findings do not exclude an important role for wind in setting the large-scale circulation. In particular, the layer thickness of inflowing AW and the level of no motion (or equivalently,

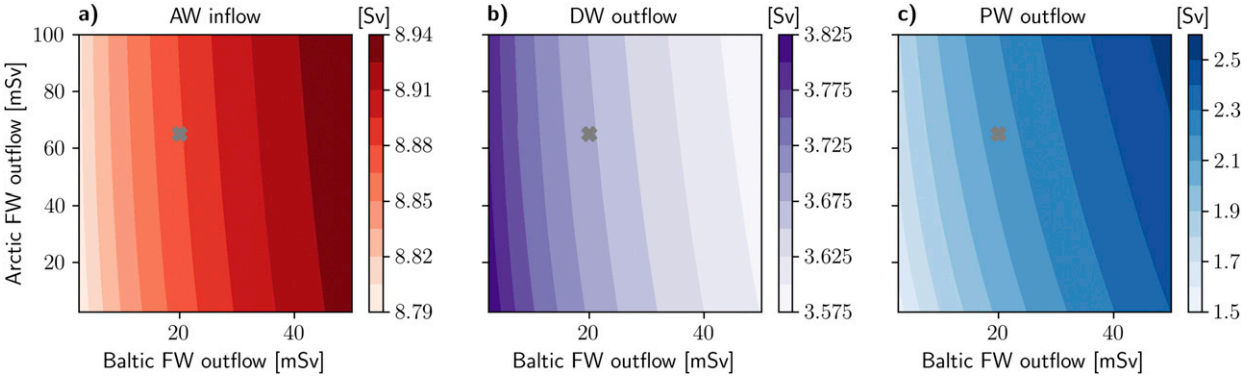

FIG. 15. Relative impact of Arctic and Baltic freshwater outflows. (a) AW inflow $\Psi_1(x = 0)$, (b) DW outflow $\Psi_1(x = L)$, and (c) PW outflow $\Psi_2(x = L)$. Gray crosses indicate present-day values of Arctic and Baltic freshwater outflows.

the bottom velocity) are likely dependent on the large-scale wind field. Wind is also likely to be important for forcing circulation along closed f/H contours (Nøst and Isachsen 2003), whereas the present model only describes circulation along open f/H contours. Finally, potential vorticity dynamics are important as well (Yang and Price 2007), although in the present study implicit mixing prevents conservation of potential vorticity.

Aforementioned studies can largely be classified in two groups based on their approach to water mass transformation. A number of these have described a single water mass with downstream modified properties (e.g., Walin et al. 2004; Spall 2004, 2012; Wåhlin and Johnson 2009). In contrast, Straneo (2006) has described the transformation of AW to a qualitatively different water mass, while retaining AW hydrography. The present model combines these approaches by allowing for the cooling of AW, as well as the net transformation of AW to both DW and PW. This approach leads to the emergence of a hydrography that qualitatively resembles observations along the eastern boundary of the Nordic seas (see Fig. 2). The model validity is limited by the length of the boundary, as a sufficiently long boundary diminishes AW transport and leads to a PW thickness that extends below the shelf break. Both of these factors introduce a change in dynamics that is not included in the present model. However, observations along the western boundary of the Nordic seas indicate that the qualitative hydrography is maintained along the complete boundary of the Nordic seas (e.g., Håvik et al. 2017).

The combined impact of coastal freshwater input and heat loss was previously addressed by Wåhlin and Johnson (2009). The present study differs from theirs in a number of ways. Most critically, we allow for the establishment of a halocline. This introduces a range of extended dynamics associated with vertical and eddy diffusion of salt, the prevention of freshwater into the Atlantic layer, and the reduction of AW transport by the formation of a coastal current. Their model describes water mass transformation in terms of a mean buoyancy of the boundary current. However, we indicate that the velocity structure and water mass transformation depend strongly on the stratification within the boundary current. Finally, in their model, the inflow strength of AW is prescribed, and water mass transformation does not impact the circulation strength.

6. Conclusions

In this study, we present a boundary current model for a coupled overturning and estuarine circulation in a marginal sea such as the Nordic seas. This circulation is characteristic for the convergence of the alpha and beta oceans between the subtropics and the polar regions. The estuarine circulation governs the production of Polar Water due to a balance between runoff and salt diffusion across a halocline which resides over the continental shelves. Eddies play a dominant role in the cross-halocline exchange, particularly in regions where a relatively deep halocline suppresses vertical diffusion. Whereas Polar Water formation is commonly attributed to processes in the Arctic Ocean, this model reveals the potentially significant contribution of runoff sources in the Nordic seas to maintaining the estuarine circulation. This model does not resolve what fraction of Polar Water is formed in the coastal regions in the Nordic seas and what fraction in the Arctic Ocean. The model does, however, describe the potential impact of Polar Water formation in the Nordic seas on the boundary current dynamics of Atlantic Water.

Runoff feeds the estuarine circulation, which in turn impacts the overturning circulation through suppression of the slope current's baroclinic instability. Ultimately, the estuarine and overturning circulations are coupled through a shared inflow of Atlantic Water. The presence of a coupled estuarine circulation has previously been shown to increase stability of an overturning circulation, making it less prone to abrupt transitions induced by freshwater input (Lambert et al. 2016). As reported by Spall (2012), an overturning circulation in a marginal sea may destabilize due to sufficient precipitation into the basin interior. The estuarine circulation described in the present study may instead lead to a more stable overturning circulation as concluded by Lambert et al. (2016).

The description of an estuarine circulation as a boundary current reveals a large variation in the potential impact of different freshwater sources on inflows and outflows into a marginal sea. Present considerations of future changes in the Nordic seas freshwater budget appear much concerned with Greenland melt and Arctic freshwater outflow. The present study suggests that the less emphasized freshwater sources in the eastern Nordic seas, and the Baltic freshwater outflow in particular, may have a surprisingly large basinwide impact despite their relatively moderate magnitude.

This dominant potential of upstream freshwater sources such as the Baltic outflow highlights the insight gained from describing water mass transformation in terms of boundary current dynamics. We have configured a model that both resembles observed circulation and hydrography in the Nordic seas and remains relatively basic so that its behavior can be physically interpreted. For this, we have made several simplifying assumptions relating to forcing and geometry. One therefore needs to take some caution with directly projecting the model to the Nordic seas, as

both Atlantic and Polar Water circulate the Arctic Ocean, where additional water mass transformation occurs.

The boundary current model presented in this study is the first of its kind to explicitly describe a marginal sea as a transition zone between regions of temperature-dominated stratification (alpha oceans) and salinity-dominated stratification (beta ocean). Projected changes in freshwater input, surface heat loss, and sea ice cover make these transition zones some of the most sensitive regions to climate change. Our findings provide an example of the interaction between the alpha and beta oceans, revealing a field of dynamics specific to transition zones, which may be essential for understanding future changes of the subpolar seas and large-scale ocean circulation.

Acknowledgments. This research was supported by the Research Council of Norway project NORTH. Support for the publication was provided by the University of Bergen. Ocean Outlook has supported a research visit for EL to Woods Hole Oceanographic Institute where much of the current work has been carried out. Support for MAS was provided by the National Science Foundation Grant OCE-1558742. The authors thank F. Straneo, H. Johnson, and I. Fer for interesting discussions on the model configuration, and we are grateful to L. Håvik and P. Haugan for useful comments on the presentation of this paper. Finally, we thank Anna Wåhlin and one anonymous reviewer for their input that greatly helped to improve this paper.

REFERENCES

Bacon, S., P. G. Myers, B. Rudels, and D. A. Sutherland, 2008: Accessing the inaccessible: Buoyancy-driven coastal currents on the shelves of Greenland and eastern Canada. *Arctic–Subarctic Ocean Fluxes*, Springer, 703–722, https://doi.org/10.1007/978-1-4020-6774-7_29.

Björk, G., B. G. Gustafsson, and A. Stigebrandt, 2001: Upper layer circulation of the Nordic seas as inferred from the spatial distribution of heat and freshwater content and potential energy. *Polar Res.*, **20**, 161–168, https://doi.org/10.3402/polar.v20i2.6513.

Blindheim, J., 1989: Cascading of Barents Sea bottom water into the Norwegian Sea. *Rapp. P.-V. Reun.- Cons. Int. Explor. Mer*, **188**, 49–58.

Boyd, T. J., and E. A. D'Asaro, 1994: Cooling of the West Spitsbergen Current: Wintertime observations west of Svalbard. *J. Geophys. Res.*, **99**, 22 597–22 618, https://doi.org/10.1029/94JC01824.

Carmack, E. C., 2007: The alpha/beta ocean distinction: A perspective on freshwater fluxes, convection, nutrients and productivity in high-latitude seas. *Deep-Sea Res. II*, **54**, 2578–2598, https://doi.org/10.1016/j.dsr2.2007.08.018.

Cottier, F. R., and E. J. Venables, 2007: On the double-diffusive and cabbeling environment of the Arctic Front, West Spitsbergen. *Polar Res.*, **26**, 152–159, https://doi.org/10.1111/j.1751-8369.2007.00024.x.

de Steur, L., E. Hansen, C. Mauritzen, A. Beszczynska-Möller, and E. Fahrbach, 2014: Impact of recirculation on the East Greenland Current in Fram Strait: Results from moored current meter measurements between 1997 and 2009. *Deep-Sea Res. I*, **92**, 26–40, https://doi.org/10.1016/j.dsr.2014.05.018.

——, R. S. Pickart, A. Macrander, K. Våge, B. Harden, S. Jónsson, S. Østerhus, and H. Valdimarsson, 2017: Liquid freshwater transport estimates from the East Greenland Current based on continuous measurements north of Denmark Strait. *J. Geophys. Res. Oceans*, **122**, 93–109, https://doi.org/10.1002/2016JC012106.

Dickson, R., B. Rudels, S. Dye, M. Karcher, J. Meincke, and I. Yashayaev, 2007: Current estimates of freshwater flux through Arctic and subarctic seas. *Prog. Oceanogr.*, **73**, 210–230, https://doi.org/10.1016/j.pocean.2006.12.003.

Eldevik, T., and J. E. Ø. Nilsen, 2013: The Arctic–Atlantic thermohaline circulation. *J. Climate*, **26**, 8698–8705, https://doi.org/10.1175/JCLI-D-13-00305.1.

Forget, G., J.-M. Campin, P. Heimbach, C. N. Hill, R. M. Ponte, and C. Wunsch, 2015: ECCO version 4: An integrated framework for non-linear inverse modeling and global ocean state estimation. *Geosci. Model Dev.*, **8**, 3071–3104, https://doi.org/10.5194/gmd-8-3071-2015.

Fukumori, I., O. Wang, I. Fenty, G. Forget, P. Heimbach, and R. M. Ponte, 2017: ECCO version 4 release 3. DSpace@MIT, accessed 18 September 2018, http://hdl.handle.net/1721.1/110380.

Haine, T. W., and Coauthors, 2015: Arctic freshwater export: Status, mechanisms, and prospects. *Global Planet. Change*, **125**, 13–35, https://doi.org/10.1016/j.gloplacha.2014.11.013.

Haney, R. L., 1971: Surface thermal boundary condition for ocean circulation models. *J. Phys. Oceanogr.*, **1**, 241–248, https://doi.org/10.1175/1520-0485(1971)001<0241:STBCFO>2.0.CO;2.

Hansen, B., and S. Østerhus, 2000: North Atlantic–Nordic seas exchanges. *Prog. Oceanogr.*, **45**, 109–208, https://doi.org/10.1016/S0079-6611(99)00052-X.

Håvik, L., R. S. Pickart, K. Våge, A. M. Thurnherr, A. Beszczynska-Möller, W. Walczowski, and W.-J. von Appen, 2017: Evolution of the East Greenland Current from Fram Strait to Denmark Strait: Synoptic measurements from summer 2012. *J. Geophys. Res. Oceans*, **122**, 1974–1994, https://doi.org/10.1002/2016JC012228.

Kuhlbrodt, T., A. Griesel, M. Montoya, A. Levermann, M. Hofmann, and S. Rahmstorf, 2007: On the driving processes of the Atlantic meridional overturning circulation. *Rev. Geophys.*, **45**, RG2001, https://doi.org/10.1029/2004RG000166.

Lambert, E., T. Eldevik, and P. M. Haugan, 2016: How northern freshwater input can stabilise thermohaline circulation. *Tellus*, **68A**, 31051, https://doi.org/10.3402/tellusa.v68.31051.

Mauritzen, C., 1996: Production of dense overflow waters feeding the North Atlantic across the Greenland-Scotland Ridge. Part 1: Evidence for a revised circulation scheme. *Deep-Sea Res. I*, **43**, 769–806, https://doi.org/10.1016/0967-0637(96)00037-4.

——, and Coauthors, 2011: Closing the loop—Approaches to monitoring the state of the Arctic Mediterranean during the International Polar Year 2007–2008. *Prog. Oceanogr.*, **90**, 62–89, https://doi.org/10.1016/j.pocean.2011.02.010.

Nilsson, J., and G. Walin, 2010: Salinity-dominated thermohaline circulation in sill basins: Can two stable equilibria exist? *Tellus*, **62A**, 123–133, https://doi.org/10.1111/j.1600-0870.2009.00428.x.

Nøst, O. A., and P. E. Isachsen, 2003: The large-scale time-mean ocean circulation in the Nordic seas and Arctic Ocean estimated from simplified dynamics. *J. Mar. Res.*, **61**, 175–210, https://doi.org/10.1357/002224003322005069.

Rudels, B., 1989: The formation of Polar Surface Water, the ice export and the exchanges through the Fram Strait. *Prog. Oceanogr.*, **22**, 205–248, https://doi.org/10.1016/0079-6611(89)90013-X.

——, 2010: Constraints on exchanges in the Arctic Mediterranean—Do they exist and can they be of use? *Tellus*, **62A**, 109–122, https://doi.org/10.1111/j.1600-0870.2009.00425.x.

Saloranta, T. M., and P. M. Haugan, 2004: Northward cooling and freshening of the warm core of the West Spitsbergen Current. *Polar Res.*, **23**, 79–88, https://doi.org/10.3402/polar.v23i1.6268.

Skagseth, Ø., K. F. Drinkwater, and E. Terrile, 2011: Wind- and buoyancy-induced transport of the Norwegian Coastal Current in the Barents Sea. *J. Geophys. Res.*, **116**, C08007, https://doi.org/10.1029/2011JC006996.

Spall, M. A., 2004: Boundary currents and watermass transformation and in marginal and seas. *J. Phys. Oceanogr.*, **34**, 1197–1213, https://doi.org/10.1175/1520-0485(2004)034<1197:BCAWTI>2.0.CO;2.

——, 2012: Influences of precipitation on water mass transformation and deep convection. *J. Phys. Oceanogr.*, **42**, 1684–1700, https://doi.org/10.1175/JPO-D-11-0230.1.

——, 2013: On the circulation of Atlantic Water in the Arctic Ocean. *J. Phys. Oceanogr.*, **43**, 2352–2371, https://doi.org/10.1175/JPO-D-13-079.1.

St-Laurent, P., F. Straneo, and D. G. Barber, 2012: A conceptual model of an Arctic sea. *J. Geophys. Res.*, **117**, C06010, https://doi.org/10.1029/2011JC007652.

Steele, M., J. H. Morison, and T. B. Curtin, 1995: Halocline water formation in the Barents Sea. *J. Geophys. Res.*, **100**, 881–894, https://doi.org/10.1029/94JC02310.

Stewart, K. D., and T. W. N. Haine, 2016: Thermobaricity in the transition zones between alpha and beta oceans. *J. Phys. Oceanogr.*, **46**, 1805–1821, https://doi.org/10.1175/JPO-D-16-0017.1.

Stigebrandt, A., 1981: A model for the thickness and salinity of the upper layer in the Arctic Ocean and the relationship between the ice thickness and some external parameters. *J. Phys. Oceanogr.*, **11**, 1407–1422, https://doi.org/10.1175/1520-0485(1981)011<1407:AMFTTA>2.0.CO;2.

——, 1985: On the hydrographic and ice conditions in the northern North Atlantic during different phases of a glaciation cycle. *Palaeogeogr. Palaeoclimatol. Palaeoecol.*, **50**, 303–321, https://doi.org/10.1016/S0031-0182(85)80019-5.

Straneo, F., 2006: On the connection between dense water formation, overturning, and poleward heat transport in a convective basin. *J. Phys. Oceanogr.*, **36**, 1822–1840, https://doi.org/10.1175/JPO2932.1.

Sutherland, D. A., and R. S. Pickart, 2008: The East Greenland coastal current: Structure, variability, and forcing. *Prog. Oceanogr.*, **78**, 58–77, https://doi.org/10.1016/j.pocean.2007.09.006.

Sverdrup, H. U., M. W. Johnson, and R. H. Fleming, 1942: *The Oceans: Their Physics, Chemistry, and General Biology*. Prentice-Hall, 1087 pp.

Visbeck, M., J. Marshall, and H. Jones, 1996: Dynamics of isolated convective regions in the ocean. *J. Phys. Oceanogr.*, **26**, 1721–1734, https://doi.org/10.1175/1520-0485(1996)026<1721:DOICRI>2.0.CO;2.

Wåhlin, A. K., and H. L. Johnson, 2009: The salinity, heat, and buoyancy budgets of a coastal current in a marginal sea. *J. Phys. Oceanogr.*, **39**, 2562–2580, https://doi.org/10.1175/2009JPO4090.1.

Walczowski, W., 2013: Frontal structures in the West Spitsbergen Current margins. *Ocean Sci.*, **9**, 957–975, https://doi.org/10.5194/os-9-957-2013.

Walin, G., G. Broström, J. Nilsson, and O. Dahl, 2004: Baroclinic boundary currents with downstream decreasing buoyancy: A study of an idealized Nordic seas system. *J. Mar. Res.*, **62**, 517–543, https://doi.org/10.1357/0022240041850048.

Werenskiold, W., 1935: Coastal currents. *Geofys. Publ.*, **10** (13), 1–14, http://www.ngfweb.no/docs/NGF_GP_Vol10_no13.pdf.

Whitney, M. M., and R. W. Garvine, 2005: Wind influence on a coastal buoyant outflow. *J. Geophys. Res.*, **110**, C03014, https://doi.org/10.1029/2003JC002261.

Winsor, P., J. Rodhe, and A. Omstedt, 2001: Baltic Sea ocean climate: An analysis of 100 yr of hydrographic data with focus on the freshwater budget. *Climate Res.*, **18**, 5–15, https://doi.org/10.3354/cr018005.

Yang, J., and J. F. Price, 2007: Potential vorticity constraint on the flow between two basins. *J. Phys. Oceanogr.*, **37**, 2251–2266, https://doi.org/10.1175/JPO3116.1.